

Modulation-induced long-range magnon bound states in one-dimensional optical lattices

Wenjie Liu^{1,2}, Yongguan Ke^{1,3}, Bo Zhu¹, Chaohong Lee^{1,2,4}

¹Guangdong Provincial Key Laboratory of Quantum Metrology and Sensing & School of Physics and Astronomy, Sun Yat-Sen University (Zhuhai Campus), Zhuhai 519082, China

²State Key Laboratory of Optoelectronic Materials and Technologies, Sun Yat-Sen University (Guangzhou Campus), Guangzhou 510275, China

³Nonlinear Physics Centre, Research School of Physics, Canberra ACT 2601, Australia

⁴Synergetic Innovation Center for Quantum Effects and Applications, Hunan Normal University, Changsha 410081, China

E-mail: lichaoh2@mail.sysu.edu.cn

Abstract. Ultracold two-level atoms in optical lattices offer an excellent experimental platform to explore magnon excitations [Fukuhara *et al* 2013 *Nat. Phys.* **9**, 235; Fukuhara *et al* 2013 *Nature* **502**, 76]. Here, we investigate how gradient magnetic field and periodically modulated tunneling strength affect the two-magnon excitations in these ultracold atomic systems. In the resonant condition where the driving frequency matches and smooths the potential bias, the system gains translational invariance in both space and time in the rotating frame, and thus we can develop a Floquet-Bloch band theory for two magnons. We find a new kind of bound states with relative distance no less than two sites, apart from the conventional bound states with relative distance at one site, which indicates the modulation-induced long-range interaction. We analytically derive an effective Hamiltonian via the many-body perturbation theory for a deeper understanding of such novel bound states and explore the interplay between these two types of bound states. Moreover, we propose to probe modulation-induced bound states via quantum walks. Our study not only provides a scheme to form long-range magnon bound states, but also lays a cornerstone for engineering exotic quantum states in multi-particle Floquet systems.

Keywords: ultracold atoms in optical lattices, magnon bound states, Floquet-Bloch band

1. Introduction

Periodic modulations in quantum systems have attracted tremendous interests and attentions in recent years [1, 2, 3, 4, 5, 6, 7]. Periodic modulation not only provides a versatile tool to manipulate the quantum particles, but also brings novel states of matter into the quantum systems [8]. It has already been applied to control the hopping [9, 10], band structure [11, 12], and quantized transport of a single particle [13, 14, 15, 16, 17, 18]. Remarkably, artificial gauge field [19] and Floquet topological insulator [20, 21, 22] have been realized by well-designed modulation protocols. In principle, Floquet-Bloch theory of a single particle has been well developed to analyze the properties of periodically modulated systems [23]. However, many-body effects induced by time modulations are more challenging and appealing. Some novel Floquet many-body states, such as collective emission of matter-wave jets [24], have been realized in ultracold atomic systems.

Optical lattice of ultracold atoms, known as an excellent simulator, enables flexible engineering of dynamical modulations [25] as well as precise controlling of atom-atom interactions [26, 27]. Owing to the excellent experimental techniques, it becomes possible to periodically modulate many-body systems with various methods. Considering Hubbard-type models, periodic modulation of tunneling is used for engineering the interaction [28, 29]. Modulation of both on-site energy and interaction is a route to create the nearest-neighbor (NN) interaction and density-assisted tunneling [30]. Tunable three-body interaction was predicted to support fractional quantum hall states [31]. Remarkably, density-dependent correlated tunneling [32] and density-dependent synthetic gauge fields [33] have already been observed in optical lattices of cold atoms.

Optical lattice of ultracold atoms is also an ideal platform to simulate magnon excitations in a spin chain. The dynamics of single magnon and two-magnon bound states in an undriven spin chain have been observed in ultracold atomic experiments [34, 35]. Motivated by these pioneer works, the studies of spin models have attracted broad interests in recent years [36, 37, 38]. Interestingly, periodically driven gradient magnetic field in a spin chain is supposed to tune long-range interaction to short-range interaction [39]. It is meaningful to engineer novel interactions in a time-modulated tilted spin chain with ultracold atoms. Furthermore, it is also well worth exploring the correlation properties arising from the engineered interactions and the way to probe the engineered interactions.

In this paper, we study two strongly interacting magnons in a spin chain under a gradient magnetic field and periodic modulation of hopping, which can be realized in a one-dimensional optical lattice of cold atoms. When the potential bias between NN sites is equal to the driving frequency, a single magnon can resonantly tunnel to the neighboring sites. We develop a Floquet-Bloch band theory for two magnons, because the system in the rotating frame is invariant when the two magnons are shifted as a whole by multiples of lattice constant and time period. Apart from

conventional bound states, we find that two magnons are bounded within two sites by calculating the magnon-magnon correlation, indicating effective next-nearest-neighbor (NNN) interactions. An effective two-magnon model is obtained by using the many-body perturbation theory, which interprets the physical mechanism of modulation-induced long-range bound states. The effective NNN interaction can be tuned to be positive or negative. When the NN interaction equals to the modulation frequency, there exists a resonance between the bound states with relative one-site and two-site distances. Considering the experimental realization, we also propose to probe the effective long-range two-magnon bound states via the quantum walks.

This paper is organized as follows. In Sec. 2, we briefly describe the realization of driven two-magnon model. In Sec. 3, we calculate the quasienergy spectrum as a function of NN interaction, by using the Floquet spectrum analysis in both time and frequency domains. In Sec. 4, we analyze the Floquet-Bloch band, derive an effective two-magnon model for the modulation-induced long-range bound states, and show the resonance between two kinds of bound states. In Sec. 5, we verify the long-range two-magnon bound states via the quantum walks. In Sec. 6, we give a brief summary and discussion.

2. Model

Owed to current experiment techniques in manipulating ultracold atoms, single magnon and magnon bound states can be created by loading two-level atoms in a one-dimensional optical lattice [34, 35]. One may label the two hyperfine levels of atoms as spin up $|\uparrow\rangle$ and spin down $|\downarrow\rangle$. Through applying a gradient magnetic field, spin up and spin down feel opposite potentials at the l -th site, $V_{l\uparrow} = -V_{l\downarrow} = lB$ with the gradient B . The Hamiltonian reads

$$\begin{aligned} \hat{H}_{\text{BH}} = & - \sum_{\langle l,g \rangle, \sigma=\uparrow, \downarrow} t_{\sigma} \hat{b}_{l\sigma}^{\dagger} \hat{b}_{g\sigma} + \sum_{l\sigma} \frac{U_{\sigma\sigma}}{2} \hat{n}_{l\sigma} (\hat{n}_{l\sigma} - 1) \\ & + U_{\uparrow\downarrow} \sum_l \hat{n}_{l\uparrow} \hat{n}_{l\downarrow} + \sum_{l\sigma} V_{l\sigma} \hat{n}_{l\sigma}. \end{aligned} \quad (1)$$

Here, $\sigma = \uparrow, \downarrow$, $\hat{b}_{l\sigma}^{\dagger}$ ($\hat{b}_{l\sigma}$) is the particle creation (annihilation) operator, $\hat{n}_{l\sigma}$ is the number operator, t_{σ} is the hopping strength of $|\sigma\rangle$, and $U_{\sigma\sigma'}$ is the interaction strength between $|\sigma\rangle$ and $|\sigma'\rangle$.

In the Mott-insulator regime with one boson atom per site, one can define the spin-1/2 operators $\hat{S}_l^{\mathcal{I}}$ ($\mathcal{I} = x, y, z$) as

$$\begin{aligned} \hat{S}_l^+ &= \hat{b}_{l\uparrow}^{\dagger} \hat{b}_{l\downarrow}, \\ \hat{S}_l^- &= \hat{b}_{l\downarrow}^{\dagger} \hat{b}_{l\uparrow}, \\ \hat{S}_l^z &= (\hat{n}_{l\uparrow} - \hat{n}_{l\downarrow})/2. \end{aligned} \quad (2)$$

Introducing the spin raising and lowering operators $\hat{S}_l^{\pm} = \hat{S}_l^x \pm i\hat{S}_l^y$ and the parameters

$$J = \frac{2t_{\uparrow}t_{\downarrow}}{U_{\uparrow\downarrow}}, \Delta = \frac{4t_{\uparrow}^2}{U_{\uparrow\uparrow}} + \frac{4t_{\downarrow}^2}{U_{\downarrow\downarrow}} - \frac{2(t_{\uparrow}^2 + t_{\downarrow}^2)}{U_{\uparrow\downarrow}}, \quad (3)$$

one can obtain a Heisenberg XXZ chain,

$$\hat{H} = \sum_{l=-L}^L (J(t)\hat{S}_l^+ \hat{S}_{l+1}^- + \text{H.c.} + \Delta \hat{S}_l^z \hat{S}_{l+1}^z + lB \hat{S}_l^z). \quad (4)$$

Here, the total chain length is $L_t = 2L + 1$. Below we focus on the case of periodically modulated parameter, $J(t) = (J_0 + J_1 \cos(\omega t))/2$ with the d.c amplitude J_0 , the a.c amplitude J_1 and the modulation frequency ω . Unlike the three-color modulations in the Fermi-Hubbard model [29], our Heisenberg XXZ chain (4) only involves a single frequency. For simplicity, we choose the units of $J_0 = \hbar = 1$. The longitudinal spin-exchange coupling Δ can be tuned by Feshbach resonance [26, 27] and we assume $\Delta \geq 0$. The magnetic field gradient B breaks the translational symmetry of the system. The ground state is the fully ferromagnetic state $|\downarrow\downarrow\downarrow \dots \downarrow\rangle$ for a positive and sufficiently large B . By flipping spins over the ground state $|\downarrow\downarrow\downarrow \dots \downarrow\rangle$, we obtain the excited states. Once one considers the ground state $|\downarrow\downarrow\downarrow \dots \downarrow\rangle$ as a vacuum state, magnon can be regarded as the basic excitation around the ferromagnetic ground state. Considering the mapping relations $|\downarrow\rangle \leftrightarrow |0\rangle, |\uparrow\rangle \leftrightarrow |1\rangle, \hat{S}_l^+ \leftrightarrow \hat{a}_l^\dagger, \hat{S}_l^- \leftrightarrow \hat{a}_l$, and $\hat{S}_l^z \leftrightarrow \hat{n}_l - \frac{1}{2}$, it amounts to load magnons into the tilted optical lattice with periodically driven hopping rate and NN interaction, i.e., $\hat{H} = \sum_l \left(\frac{J(t)}{2} \hat{a}_l^\dagger \hat{a}_{l+1} + \text{H.c.} + \Delta \hat{n}_l \hat{n}_{l+1} + Bl \hat{n}_l \right)$. \hat{a}_l^\dagger (\hat{a}_l) creates (annihilates) a magnon at site l and satisfies the commutation relations of the hard-core bosons. $\hat{n}_l = \hat{a}_l^\dagger \hat{a}_l$ is the number operator.

By a unitary treatment $\hat{H}' = \hat{U} \hat{H} \hat{U}^\dagger - i \hat{U} \frac{\partial}{\partial t} \hat{U}^\dagger$ with $\hat{U} = \exp(i \sum_l l B t \hat{n}_l)$ [40, 41], the driven magnon Hamiltonian in the rotating frame is given as,

$$\hat{H}' = \sum_{l=-L}^L (J(t) e^{-iBt} \hat{a}_l^\dagger \hat{a}_{l+1} + \text{H.c.}) + \Delta \sum_{l=-L}^L \hat{n}_l \hat{n}_{l+1}. \quad (5)$$

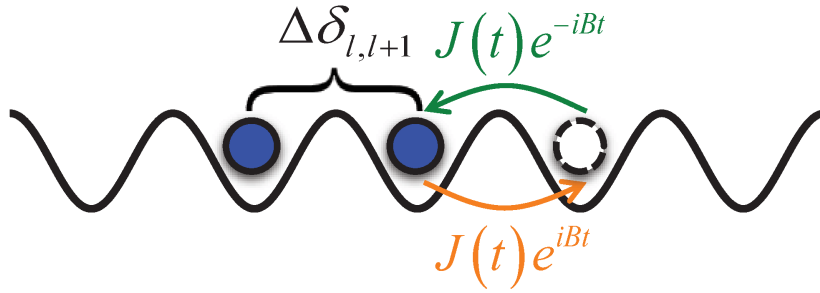
If we impose periodic boundary condition, Hamiltonian (5) preserves translational invariance, which is slightly different from Hamiltonian (4) at the boundary. We only consider the bulk properties where the tiny difference between Hamiltonian (4) and (5) takes no effect. For convenience, we focus on Hamiltonian (5) with periodic boundary condition in the following paper.

Since $[\hat{H}', \hat{n}] = 0$ with $\hat{n} = \sum_l \hat{n}_l$, the total magnon number \hat{n} is conserved. This means that subspaces with different magnon numbers are decoupled. To take magnon-magnon interaction into account, two-magnon excitation is a fundamental object and gives enlightenment to multi-magnon excitations. We aim to manipulate a NNN two-magnon bound state and explore its interplay with original NN bound state from both numerical and analytical perspectives. Based upon a two-body ansatz related to center-of-mass and relative position, we concentrate our analysis on the subspace of two-magnon excitations. The driven two-magnon model is schematically shown in figure 1(a).

In the absence of the gradient magnetic field and periodic driving ($B = J_1 = 0$), the spin-1/2 XXZ chain occurs a quantum phase transition at $\Delta = J$. For the two-magnon system, an isolated bound-state band and a continuum scattering band

appear in the energy spectrum for $\Delta > J$, while the bound-state band merges into the continuum one for $0 < \Delta < J$. After flipping two spins over the ground state with all spins downward, two magnons undergo Bloch oscillations in the presence of the gradient magnetic field [42]. Coherent delocalization occurs by introducing the resonant modulation $\omega = B$, which is potentially applied for measuring the magnetic field gradient [43, 44]. In our paper, we only consider the resonant driven condition, i.e., $\omega = B$, where photon-assisted tunneling resonances may happen [45, 46].

(a) Driven two-magnon model



(b) Effective two-magnon model

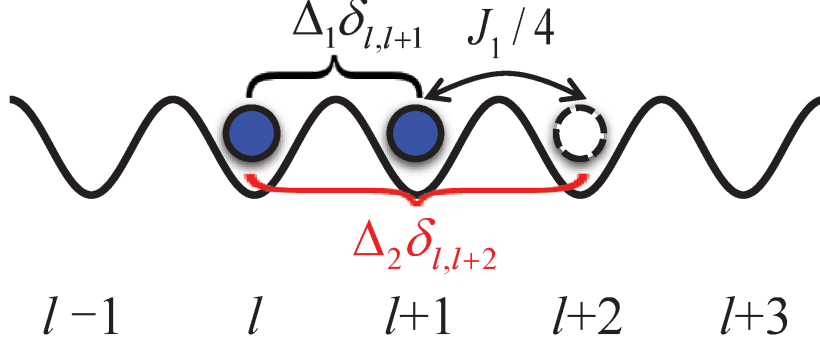


Figure 1. (Color online) (a) The driven two-magnon model (5) with NN interaction and time-modulated hopping rate. (b) The effective two-magnon model (19) with modulation-induced NNN interaction, modified NN interaction and reduced hopping rate.

3. Floquet spectrum analysis

Only NN antiferromagnetic interaction ($\Delta > 0$) is considered in the Hamiltonian (5), while our conclusions can easily be extended to the corresponding ferromagnetic one ($\Delta < 0$) due to the related symmetry analysis [42]. The interplay between NN interaction and time modulation makes it possible to induce long-range bound states. To understand how the long-range bound states come from, we need to analyze the Floquet spectrum and the quasieigenstates. There are two equivalent ways to calculate

the Floquet-Bloch spectrum, one is in the time domain and the other is in the frequency domain.

In the following sections, we aim to study the modulation-induced NNN bound state and give an effective picture for its coexistence and competition with the original NN bound state. In the subsection 3.1 and 3.2, we will respectively analyze how the Floquet spectrum changes with Δ in time and frequency domains in the high-frequency region. However, in addition to the NNN bound states, our system can also be modulated to induce other bound states. In Appendix A, we give a brief discussion on the modulation-induced bound state with relative distance at three and four sites.

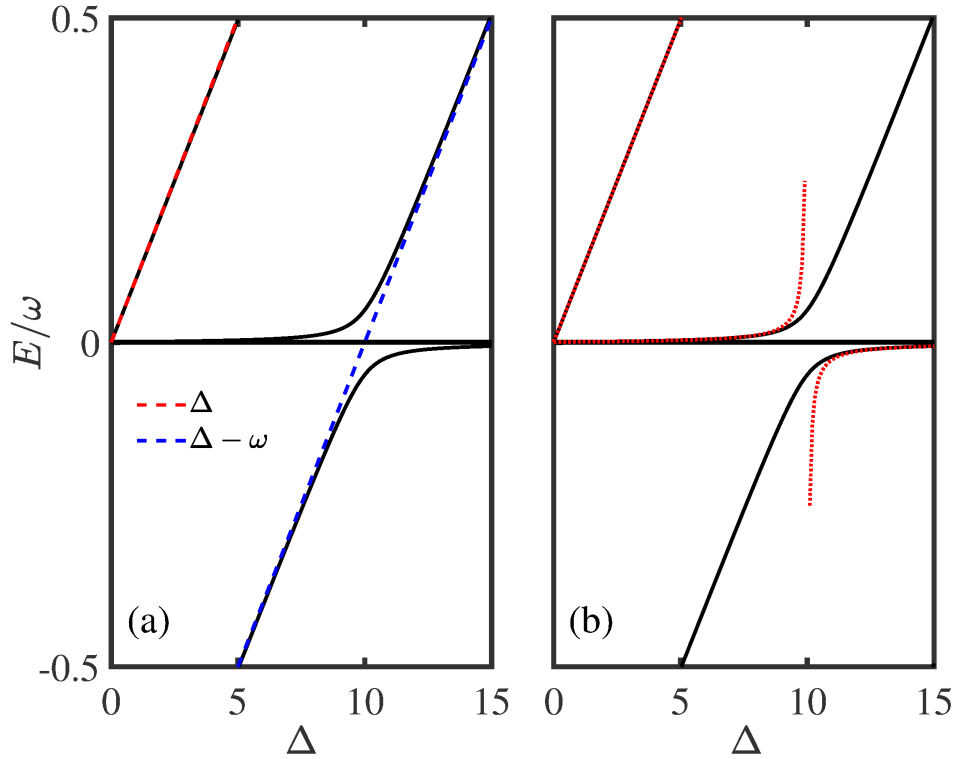


Figure 2. (Color online) (a) Quasienergy spectrum E as a function of Δ given by the static effective Hamiltonian \hat{H}_F (black solid lines). The red and blue dashed lines respectively represent Δ and $\Delta - \omega$ as a function of Δ . (b) The quasienergy spectra of the Floquet-Bloch lattice model (12) (black solid lines) and the effective two-magnon model (19) (red dotted lines) for $F = 5$. The other parameters are chosen as $\omega = B = 10$, $J_0 = 1$ and $J_1 = 0.01$.

3.1. Time-domain analysis

The driven two-magnon Hamiltonian (5) satisfies a discrete time translation symmetry, $\hat{H}(t + T) = \hat{H}(t)$ with a Floquet period $T = 2\pi/\omega$. We can define a time-evolution operator in one period as

$$\hat{U}_T = \hat{\mathcal{T}} \exp(-i \int_0^T \hat{H}'(t) dt) \equiv \exp(-i \hat{H}_F T), \quad (6)$$

where the static effective Hamiltonian

$$\hat{H}_F = \frac{i}{T} \log \hat{U}_T \quad (7)$$

governs the dynamics at stroboscopic time nT ($n = 1, 2, 3, \dots$). Before analyzing the dynamics, it is helpful to solve the eigenvalue problem, $\hat{H}_F|u_n\rangle = E_n|u_n\rangle$, where E_n and $|u_n\rangle$ are quasienergy and Floquet eigenstate, respectively. E_n can be restricted in the interval $[-\omega/2, \omega/2]$, which we term as the first Floquet-Brillouin zone. The quasienergy has a period ω and consists of replicas of that in the first Floquet-Brillouin zone. We calculate the quasienergy spectrum as a function of the NN interaction regarding the static effective Hamiltonian (7) (see figure 2(a)). The parameters are chosen as $\omega = B = 10$, $J_0 = 1$ and $J_1 = 0.01$. There is continuum flat band around zero energy, with eigenstates regarded as the scattering states. When $J_0, J_1 \ll \Delta$, two magnons at the NN sites approximate the bound states with energy $\sim \Delta$. The red dashed line Δ as a function of Δ is added in figure 2(a), which is well fitting with an isolated band in quasienergy spectrum (black solid lines) of \hat{H}_F . Thus, there is one isolated band $\sim \Delta$ corresponding to bound state with relative distance as 1 in quasienergy spectrum of \hat{H}_F . It becomes clearer that $\Delta - \omega$ (blue dashed line) is the replica of Δ (red dashed line). Around the resonant condition $\Delta - \omega = 0$, the bound-state band $\Delta - \omega$ (blue dashed line) is completely different from the quasienergy spectrum (black solid lines) of \hat{H}_F and mixes with the continuum band, and two isolated bands appear in the quasienergy spectrum of \hat{H}_F (see figure 2(a)). Thus, the two isolated bands around $\Delta - \omega \approx 0$ must be a modulation-induced effect.

3.2. Frequency-domain analysis

We can equivalently analyze the quasienergy spectrum in the frequency domain. The arbitrary two-magnon states can be expanded as $|\Psi\rangle = \sum_{l_1 < l_2} \psi_{l_1 l_2} |l_1 l_2\rangle$, with probability amplitudes $\psi_{l_1 l_2} = \langle \mathbf{0} | \hat{a}_{l_2} \hat{a}_{l_1} | \Psi \rangle$ for one magnon at the l_1 -th site and the other at the l_2 -th site. After substituting the two-magnon state in the Fock basis into the Schrödinger equation

$$i \frac{d}{dt} |\Psi(t)\rangle = \hat{H}' |\Psi(t)\rangle, \quad (8)$$

the amplitude probability $\psi_{l_1 l_2}(t)$ at instantaneous time t satisfies

$$\begin{aligned} i \frac{\partial}{\partial t} \psi_{l_1 l_2}(t) = & M(t)(\psi_{l_1, l_2+1} + \psi_{l_1+1, l_2}(t)) + M^*(t)(\psi_{l_1, l_2-1}(t) + \psi_{l_1-1, l_2}(t)) \\ & + \Delta \delta_{l_1, l_2 \pm 1} \psi_{l_1 l_2}(t) \end{aligned} \quad (9)$$

with $M(t) = J_1/4 + J_0/2e^{-i\omega t} + J_1/4e^{-i2\omega t}$. Considering the periodic boundary condition, we have $\psi_{l_1, l_2+L_t} = \psi_{l_1+L_t, l_2} = \psi_{l_1, l_2}$. Due to the time periodicity, we can express the probability amplitudes $\psi_{l_1 l_2}(t)$ by the Fourier components $\psi_{l_1 l_2}(t) = e^{-iEt} \sum_{\chi=-\infty}^{\infty} e^{-i\chi\omega t} U_{l_1, l_2, \chi}$ [10, 23]. Then we have

$$|\Psi(t)\rangle = e^{-iEt} \sum_{l_1 < l_2, \chi} e^{-i\chi\omega t} U_{l_1, l_2, \chi} |l_1, l_2, \chi\rangle \quad (10)$$

where $|U_{l_1, l_2, \chi}|^2$ is the probability distributing in the Floquet state $|l_1, l_2, \chi\rangle$. χ is the Floquet index taking values from $-\infty$ to ∞ . The Floquet state $|l_1, l_2, \chi\rangle$ intuitively represents two particles living in real space and Floquet space. Due to the particle conservation, the two particles always share a common χ , that is, the two particles transfer from χ to χ' as a bounded pair. Replacing the state (10) into the Eq. (8) and averaging it over one period, we can obtain

$$EU_{l_1, l_2, \chi} = (\Delta\delta_{l_1, l_2 \pm 1} - \chi\omega)U_{l_1, l_2, \chi} + \sum_q \mathcal{J}_q (U_{l_1, l_2+1, \chi-q} + U_{l_1+1, l_2, \chi-q} + U_{l_1, l_2-1, \chi+q} + U_{l_1-1, l_2, \chi+q}) \quad (11)$$

with $\mathcal{J}_0 = \mathcal{J}_2 = J_1/4$ and $\mathcal{J}_1 = J_0/2$. It is equal to a Floquet-Bloch lattice model,

$$\hat{H}_{FB} = \hat{H}_{FB}^0 + \hat{H}_{FB}^1, \quad (12)$$

with

$$\hat{H}_{FB}^0 = \sum_{l_1, l_2, \chi} (\Delta\delta_{l_1, l_2 \pm 1} - \chi\omega) |l_1, l_2, \chi\rangle \langle l_1, l_2, \chi| \quad (13)$$

and

$$\begin{aligned} \hat{H}_{FB}^1 = & \sum_{l_1, l_2, \chi, q} (\mathcal{J}_q |l_1, l_2, \chi\rangle \langle l_1, l_2 + 1, \chi - q| + \text{H.c.}) \\ & + \sum_{l_1, l_2, \chi, q} (\mathcal{J}_q |l_1, l_2, \chi\rangle \langle l_1 + 1, l_2, \chi - q| + \text{H.c.}). \end{aligned} \quad (14)$$

The Floquet index χ labels the extra dimension. We establish an equivalence between a periodically driven two-magnon model (5) and the Floquet-Bloch lattice model (12). The motion of two magnons on the periodically driven one-dimensional lattice in figure 1(a) is equivalent to the time-independent hopping dynamics of two magnon on a two-dimensional lattice model with a potential energy gradient along the χ direction. Here, \hat{H}_{FB}^0 consists of the NN interaction and the potential gradient $-\chi\omega$ along χ direction. \hat{H}_{FB}^1 consists of individual hopping of magnons in the same χ and pair-hopping between χ and χ' with $\chi' = \chi \pm 1$, $\chi \pm 2$.

Numerically, we can calculate the quasienergy spectrum by truncating the Floquet spaces ranging from $\chi = -f$ to f , and the total truncation number $F = 2f + 1$. Generally, f can be ranging from $-\infty$ to ∞ . In the high-frequency case, $\omega \gg J_0, J_1$, the energy barrier between χ and $\chi \pm 1$ is so large that the two magnons tends to localize at a few χ . A small truncation number gives sufficiently exact results and enables us to apply the perturbation theory to obtain an effective Hamiltonian. However, as the modulation frequency decreases, the wave function become spread over a larger range of χ , and a larger truncation number is needed. By choosing the same parameters as figure 2(a) and $F = 5$, we also calculate the quasienergy spectrum with the change of Δ given by the Floquet-Bloch lattice model (12) (black solid lines) in figure 2(b). Compared with the quasienergy spectrum of \hat{H}_F (black solid lines) in figure 2(a) and \hat{H}_{FB} (black solid lines) in figure 2(b), they are almost the same. It means that these two methods are equivalent. However, the analysis in the frequency domain is a more

powerful method to understand the emergence of modulation-induced isolated bands more deeply. Based on the analysis in the frequency domain, we will analyze the Bloch states under a periodic boundary condition far away and around the resonant parameter.

4. Two-body Floquet-Bloch band

In this section, we derive a Floquet-Bloch lattice model which has cotranslational symmetry along the real space but violates such symmetry along the Floquet space due to the effective potential gradient $-\chi\omega$. Thus, we can apply the many-body Bloch theorem in the real space and leave alone the Floquet index χ . Remarkably, we obtain two-body Floquet-Bloch band, a significant analysis of the many-body Bloch theorem to the periodically modulated system. Away from the resonant condition $\Delta - \omega = 0$, we analyze the isolated Floquet-Bloch bands and reveal the modulation-induced long-range two-magnon bound states. Such process can also be perfectly captured by an effective Hamiltonian via the many-body perturbation theory. Near the resonant condition, we find the hybrid of two kinds of bound states.

4.1. Modulation-induced long-range two-magnon bound states

Imposing periodic boundary condition, the Floquet-Bloch lattice model (12) is invariant by shifting the two magnons as a whole in the real space. Naturally, we introduce the center-of-mass and relative positions $R = (l_1 + l_2)/2$ and $r = l_1 - l_2$, respectively. The center-of-mass quasimomentum K is a conserved quantity. According to the many-body Bloch theorem, the wave-function is a Bloch wave along the coordinate of center-of-mass position, i.e., $U_{l_1, l_2, \chi} = e^{iKR} \phi_\chi(r)$ where $\phi_\chi(r)$ is the amplitude depending on the relative position r and the Floquet position χ . It is difficult to assume such ansatz for three or more magnon excitations.

Substituting the above ansatz into Eq. (12), the amplitude $\phi_\chi(r)$ satisfies the following eigenequation in the quasimomentum space,

$$E\phi_\chi(r) = \sum_q \mathcal{J}_q^K (\phi_{\chi-q}(r-1) + \phi_{\chi-q}(r+1)) + (\Delta\delta_{r,\pm 1} - \chi\omega)\phi_\chi(r) \quad (15)$$

with $\mathcal{J}_0^K = J_1/2 \cos(K/2)$, $\mathcal{J}_{\pm 1}^K = J_0/2 e^{\pm iK/2}$ and $\mathcal{J}_{\pm 2}^K = J_1/4 e^{\pm iK/2}$. Under the periodic boundary condition, we find $e^{iKL_t} = 1$ and $\phi_\chi(r + L_t) = e^{iKL_t/2} \phi_\chi(r)$ with $K = 2\pi\alpha/L_t$ for $\alpha = -L, -L+1, \dots, L$. Moreover, since the magnons are hard-core bosons, we have $\phi_\chi(0) = 0$ and $\phi_\chi(r) = \phi_\chi(-r)$.

Solving the above eigenequation (15), we can obtain the two-body Floquet-Bloch bands vs. K in figure 3 (more results for longer-range bound states are shown in Appendix A). The parameters are chosen as $\omega = B = 10$, $J_0 = 1$, $J_1 = 0.01$, and Δ are chosen at the left- and right-hand sides of the resonant point as $\Delta = 7, 13$ for figures 3(a) and (b), respectively. At the left-hand side of the resonant point, there are two isolated bands above a continuum band which ranges from $-|J_1|$ to $|J_1|$ (see figure 3(a)). This is qualitatively different from a conventional two-band energy spectrum of two-magnon

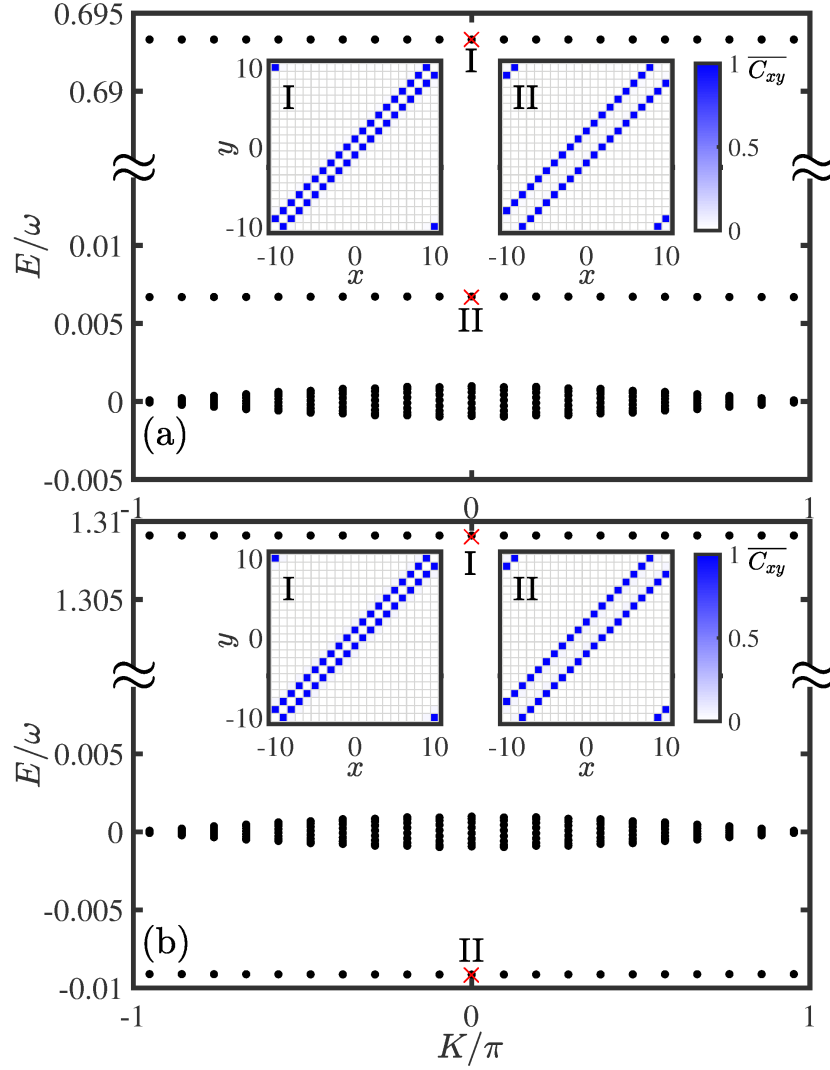


Figure 3. (Color online) Quasienergy spectrum E vs. center-of-mass momentum K away from the resonant condition for (a) $\Delta - \omega = -3$ and (b) $\Delta - \omega = 3$. The insets I and II respectively describe the normalized magnon-magnon correlations $\overline{C_{xy}} = C_{xy}/C_{xy}^{max}$ of Floquet states labeled in the isolated bands. The other parameters are chosen as $\omega = B = 10$, $J_0 = 1$ and $J_1 = 0.01$.

excitations in NN interaction quantum spin chains without the periodic driving [47]. The extra band appears with quite a similar structure to the bound-state band arising from the NN interaction. While at the right-hand side of the resonant point, the two isolated bands sandwich the continuum band (see figure 3(b)). It will be clear later that the difference between figures 3(a) and (b) relates to the positive and negative values of the effective interaction. A suitable choice of parameters results in a negative modulation-induced bound band below the continuum band.

To better understand the band structure, it is instructive to calculate the magnon-magnon correlations of corresponding Floquet states labeled I and II in figure 3. The magnon-magnon correlation is defined as $C_{xy} = \langle \Psi(T) | \hat{a}_x^\dagger \hat{a}_y^\dagger \hat{a}_y \hat{a}_x | \Psi(T) \rangle$ where $|\Psi(T)\rangle$

is the Floquet state with a given quasimomentum K . x and y take values from $-L$ to L . The magnon-magnon correlations at two specific lines $x = y \pm d$ in the (x, y) plane serve as a sensitive evidence of the two-magnon bound states, where d depends on the specific magnon-magnon interactions. For example, due to the NN interaction, the Floquet state marked with I is well distributed among the minor-diagonal lines $x = y \pm 1$ of the magnon-magnon correlations in the inset I of figure 3. While for the Floquet state marked with II, the inset II of figure 3 shows the magnon-magnon correlations are mainly distributed in the next-minor-diagonal lines. The type II Floquet state indicates the existence of effective long-range bound states. The correlation properties of the other Floquet states in these two bands are similar to their Floquet states with quasimomentum $K = 0$. They are characteristic signatures of two types of bound-state bands, respectively derived from the NN interaction and NNN interaction. Thus, we can claim the existence of modulation-induced long-range bound states.

4.2. Effective two-magnon model

Below particular attention is paid to attain an effective two-magnon model for understanding and interpreting the origination of the modulation-induced long-range bound states. Given the perturbation conditions $|\Delta - \omega| \gg J_0/2$ and $|\Delta - 2\omega| \gg J_1/4$, we divide the Floquet-Bloch lattice model (12) into two parts, \hat{H}_{FB}^0 as a dominate term and \hat{H}_{FB}^1 as a perturbed term. In the high-frequency region, $\omega \gg J_0, J_1$, it is sufficient to just take into account the five χ with $\chi = 0, \pm 1, \pm 2$. The unperturbed term \hat{H}_{FB}^0 is separated into two subspaces \mathcal{U} and \mathcal{V} . The subspace \mathcal{U} includes two kinds of states: (i) $E_P = \Delta$ for the states $\{|l, l+1, 0\rangle\}$ with $-L \leq l \leq L$ and (ii) $E_P = 0$ for the states $\{|l_1, l_2, 0\rangle\}$ with $l_1 \neq l_2 - 1, -L \leq l_1 < l_2 \leq L$. The complementary subspace \mathcal{V} consists of (iii) $E_S = \Delta - \chi\omega$ for the states $\{|l, l+1, \chi\rangle\}$ with $-L \leq l \leq L$ and (iv) $E_S = -\chi\omega$ for the states $\{|l_1, l_2, \chi\rangle\}$ with $l_1 \neq l_2 \pm 1, -L \leq l_1 < l_2 \leq L$ for $\chi = \pm 1, \pm 2$. The project operators are defined as $\hat{P} = \sum_{l_1 l_2} |l_1, l_2, 0\rangle \langle l_1, l_2, 0|$ onto \mathcal{U} and $\hat{S} = 1 - \hat{P}$ onto \mathcal{V} . We calculate the effective two-magnon model $\hat{H}_{Eff} = \hat{h}_0 + \hat{h}_1 + \hat{h}_2$ via a perturbative expansion up to the second order. In the lowest order and first order, we have

$$\hat{h}_0 = E_P \hat{P} = \Delta \sum_l |l, l+1, 0\rangle \langle l, l+1, 0| \quad (16)$$

and

$$\begin{aligned} \hat{h}_1 &= \hat{P} \hat{H}_{FB}^1 \hat{P} \\ &= \frac{J_1}{4} \sum_{l_1 l_2} (|l_1, l_2, 0\rangle \langle l_1, l_2 + 1, 0| + \langle l_1 + 1, l_2, 0| + \text{H.c.}), \end{aligned} \quad (17)$$

which respectively retain the original NN interaction Δ and NN tunneling in $\chi = 0$. For simplicity, we respectively label the eigenstates and eigenvalues of the unperturbed term \hat{H}_{FB}^0 as $\{|i\rangle\}$ and E_i , and $\{|p\rangle\}$ represent states in the subspace \mathcal{U} . The second-order

effective Hamiltonian reads

$$\begin{aligned}\hat{h}_2 &= \sum_{i_1 i_3 \in i_p, i_2 \notin i_p} \frac{J_{i_1 i_2 i_3}^{Eff}}{2} |i_1\rangle \langle i_1| \hat{H}_{FB}^1 |i_2\rangle \langle i_2| \hat{H}_{FB}^1 |i_3\rangle \langle i_3| \\ &= -\Delta_2 \sum_l (|l, l+1, 0\rangle \langle l, l+1, 0| - |l, l+2, 0\rangle \langle l, l+2, 0|)\end{aligned}\quad (18)$$

with $J_{i_1 i_2 i_3}^{Eff} = (1/(E_{i_1} - E_{i_2}) + 1/(E_{i_3} - E_{i_2}))$ and $\Delta_2 = J_0^2 \Delta / [2(\omega^2 - \Delta^2)] + J_1^2 \Delta / [8(4\omega^2 - \Delta^2)]$. Interestingly, the second-order process not only contributes to the NNN interaction, but modifies the original NN interaction. Since the high-order term is much smaller than the second-order one in the perturbation parameter region, it allows us to ignore the results beyond the second-order term.

By means of the perturbation theory [48, 49, 50], the effective two-magnon model up to second order in $\chi = 0$ is given as

$$\hat{H}_{Eff} = \frac{J_1}{4} \sum_l (\hat{a}_l^\dagger \hat{a}_{l+1} + \text{H.c.}) + \sum_{s=1,2;l} \Delta_s \hat{n}_l \hat{n}_{l+s} \quad (19)$$

with $\Delta_1 = \Delta - \Delta_2$. $\sum_l \hat{n}_l = 2$ restricts \hat{H}_{Eff} to the two-magnon sector. The effective two-magnon model (19) can be schematically described in figure 1(b) with the renormalized parameters. The effective NNN interaction comes from the asymmetric pathways between absorbing and consequently emitting phonons, $\{|l_2 - l_1 = 2, 0\rangle \rightarrow |l_2 - l_1 = 1, +\chi\rangle \rightarrow |l_2 - l_1 = 2, 0\rangle, \chi \neq 0\}$ and the inverse process, $\{|l_2 - l_1 = 2, 0\rangle \rightarrow |l_2 - l_1 = 1, -\chi\rangle \rightarrow |l_2 - l_1 = 2, 0\rangle, \chi \neq 0\}$. This is the origin of NNN interactions in a periodically modulated interacting system. The hopping rate is reduced to $J_1/4$. It must be pointed out that modulation amplitude J_1 determines the width of the continuum band $[-|J_1|, |J_1|]$. Once J_1 is sufficiently large, the NNN-interaction bound-state band may not be enough to completely separate from the continuum band. With the effective two-magnon model (19), we can systematically create and control the NNN interaction. The long-range two-magnon bound states arising from the modulation-induced NNN interaction constitutes the central idea of our paper.

To show the concreteness, we compare the quasienergy spectrum given by the effective two-magnon model (19) and that given by \hat{H}_{FB} , respectively see the red dotted and black solid lines in figure 2(b). It is clear that the isolated bands are well consistent in the perturbation parameter regime $|\Delta - \omega| \gg J_0/2$ and $|\Delta - 2\omega| \gg J_1/4$. The perturbation conditions mean the energy gap between subspaces \hat{P} and \hat{S} should be much larger than their tunneling rate. This energy gap decreases as Δ approaches to ω , so that the perturbation condition is no longer satisfied and the effective two-magnon model (19) is invalid. As shown in figure 2(b) (red dotted lines), the isolated bound band of \hat{H}_{Eff} is no longer fitting with the modulation-induced band of \hat{H}_{FB} when the NN interaction Δ nears the modulation frequency ω . But their continuum bands are always well consistent. In order to clearly clarify the modulation-induced bound band, we just plot the continuum band of \hat{H}_{FB} in figure 2(b).

4.3. Resonance between two types of bound states

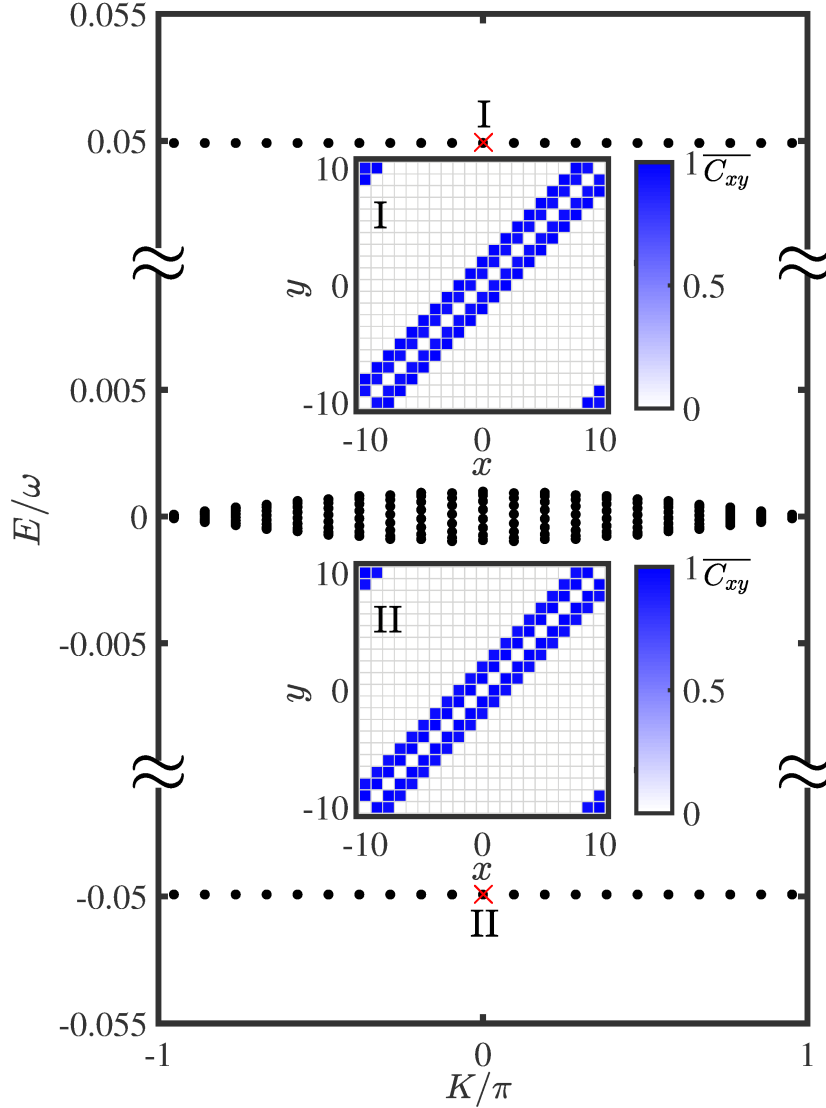


Figure 4. (Color online) Quasienergy spectrum E vs. K in the resonant condition $\Delta = \omega$. The insets I and II respectively describe the normalized magnon-magnon correlations $\overline{C_{xy}} = C_{xy}/C_{xy}^{max}$ of Floquet states labeled in the top and bottom band in the quasienergy spectrum. The other parameters are chosen as $\omega = B = 10$, $J_0 = 1$ and $J_1 = 0.01$.

However, the effective Hamiltonian (19) becomes invalid around the resonant point $\Delta = \omega$. To understand what happens in the resonant condition, we calculate the band structure and magnon-magnon correlations via the Floquet spectrum analysis in the frequency domain (see figure 4). The truncated Floquet space is limited in $\chi = 0, \pm 1, \pm 2$.

For \hat{H}_{FB}^0 , its eigenstates $\{|l, l+1, \chi\rangle : -L \leq l \leq L\}$ and $\{|l_1, l_2, \chi-1\rangle : l_1 \neq l_2-1, -L \leq l_1 < l_2 \leq L\}$ become degenerate with the energy difference $\Delta - \omega = 0$. Once

\hat{H}_{FB}^1 is added, this energy degeneracy will be broken, and these states are not longer eigenstates of the full Hamiltonian (12). Two types of bound states $|l_2 - l_1 = 1, \chi\rangle$ and $|l_2 - l_1 = 2, \chi - 1\rangle$ are coupled by a first-order process with the tunneling rate $J_0/2$, while state $|l_2 - l_1 = 1, \chi\rangle$ couples state $\{|l_2 - l_1 > 2, \chi - 1\rangle : l_1 \neq l_2 - 1, l_2 - 2\}$ by second-order or even higher-order term, which can be neglected in the high-frequency region. Here we are able to just consider the first-order tunneling process between two types of bound states $|l, l + 1, \chi\rangle$ and $|l, l + 2, \chi - 1\rangle$, then the corresponding states of the system (12) can be written as a superposition $(|l, l + 1, \chi\rangle \pm |l, l + 2, \chi - 1\rangle)/\sqrt{2}$ and the corresponding energies are $E = E_0 \pm J_0/2$.

Now we focus on the zeroth Floquet-Brillouin zone $E \in [-\omega/2, \omega/2]$, there is no energy gap between bound states $|1\rangle = |l, l + 1, 1\rangle$ and $|2\rangle = |l, l + 2, 0\rangle$ with energy $E_0 = 0$. In terms of a basis $\{|1\rangle, |2\rangle\}$, we build a two-level system with a degenerate energy E_0 . Once the first-order tunneling process $J_0/2$ is added, states $|1\rangle$ and $|2\rangle$ are not eigenstates of the full system whose eigenstates follow $|\pm\rangle = (|1\rangle \pm |2\rangle)/\sqrt{2}$ and eigenvalues are $E_0 \pm J_0/2$. The energy bands at the top and at the bottom are almost symmetrical with respect to $E_0 = 0$, and the energy gap is J_0 (see figure 4). The parameters are chosen as $J_0 = 1$, $J_1 = 0.01$ and $\Delta = \omega = 10$, in the high-frequency region $\omega \gg J_0, J_1$. We respectively mark the two Floquet states as I and II in the quasienergy spectrum and analyze their correlated properties in the insets I and II of figure 4. The top band and bottom one behave almost the same, that is, the magnon-magnon correlation is basically equal probability distribution on the minor-diagonal and next-minor-diagonal lines. These numerical results completely follow the related theoretical analysis.

There exists a process in which, with the increasing of Δ , a bound-state band caused by the NNN interaction in $\chi = 0$ emerges from the continuum band. When Δ nears ω , it gradually mixes with the bound-state band caused by the NN interaction in $\chi = 1$. The NN-interaction bound-state band in $\chi = 1$ plays a dominant role until Δ is large enough. Similarly, with the increasing of Δ , an isolated NN-interaction bound-state band of $\chi = 1$ appears below the continuum band, is mixed with the NNN-interaction one in $\chi = 0$ around the resonant point $\Delta = \omega$, and finally turns to the one of the NNN interaction in $\chi = 0$ for a sufficiently large Δ .

5. Probing long-range two-magnon bound states

Two-magnon quantum walk provides an excellent method to probe the modulation-induced long-range two-magnon bound states. It is worth to numerically simulate the dynamics of two strongly correlated magnons, initially localizing on the sites $l = -1$ and $l = 1$, which can be prepared by flipping two NNN spins from a saturated ferromagnetic state with all spins downward $|\downarrow\downarrow \dots \downarrow\rangle$. To investigate the dynamics of magnons initially locating in the bulk of the spin chain, we resort to numerically solve the time-dependent Schrödinger equation. Starting from the driven spin-1/2 Heisenberg XXZ chain under a gradient magnetic field (4), the time evolution of an arbitrary two-magnon

state $|\psi(t)\rangle$ obeys the time-dependent Schrödinger equation $i\frac{d}{dt}|\psi(t)\rangle = \hat{H}|\psi(t)\rangle$, where $|\psi(t)\rangle = \sum_{l_1 < l_2} \psi_{l_1 l_2}(t) |l_1 l_2\rangle$ and the probability amplitudes $\psi_{l_1 l_2}(t) = \langle \mathbf{0} | \hat{S}_{l_2}^- \hat{S}_{l_1}^- | \psi(t) \rangle$. With the instantaneous wave function $|\psi(t)\rangle$, we trace out the time-dependent spin

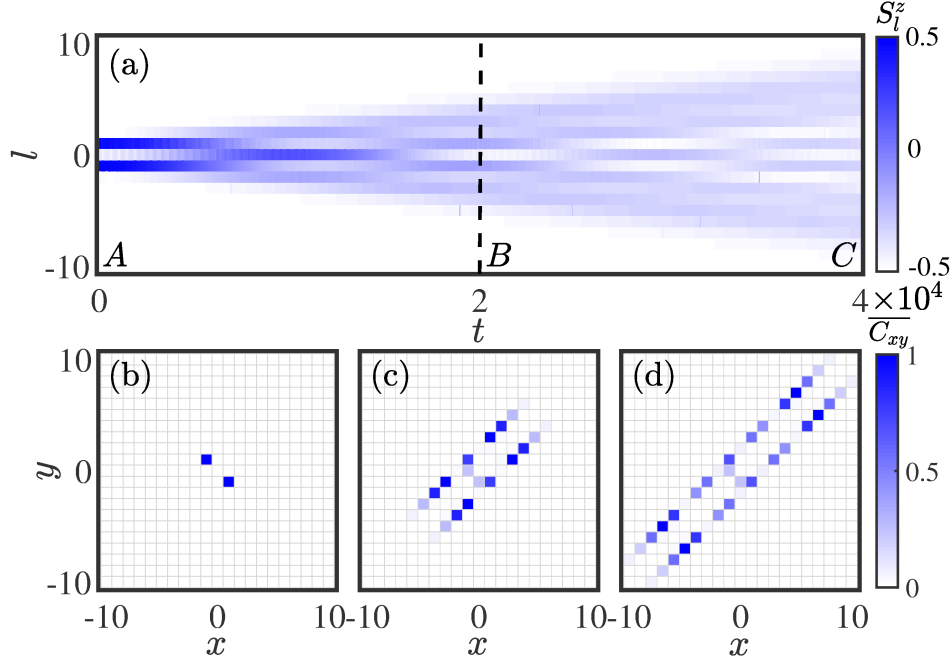


Figure 5. (Color online) Quantum walks of two magnons in the driven Heisenberg XXZ chain under a gradient magnetic field (4). (a) is the time evolution of spin distributions $S_l^z(t)$. (b), (c) and (d) are the normalized magnon-magnon correlations $\overline{C}_{xy} = C_{xy}/C_{xy}^{max}$ for different moments marked as A, B and C in (a). At the initial moment A ($t = 0$), two magnons are prepared in $|-1, 1\rangle$, so one can see two points in $(-1, 1)$ and $(1, -1)$ in (b). (c) and (d) reveal that, in the course of the time evolution, two magnons mainly move along the next-minor-diagonal lines of the magnon-magnon correlation. The parameters are chosen as $\Delta = 7$, $\omega = B = 10$, $J_0 = 1$ and $J_1 = 0.01$.

distributions $S_l^z(t) = \langle \psi(t) | \hat{S}_l^z | \psi(t) \rangle$ and the instantaneous magnon-magnon correlations $C_{xy}(t) = \langle \psi(t) | \hat{S}_x^+ \hat{S}_y^+ \hat{S}_y^- \hat{S}_x^- | \psi(t) \rangle$ for different moments, where l , x and y take values from $-L$ to L .

Figure 5 displays the time evolution of spin distributions and the corresponding instantaneous magnon-magnon correlations at three different moments for $J_0 = 1$, $J_1 = 0.01$, $\Delta = 7$, $\omega = B = 10$, and $L_t = 21$, with the periodic boundary condition. Figure 5(a) shows a light cone in the time evolution of spin distributions before the two magnons collide with the boundaries. We timely cut off the evolution of spin distributions to avoid the boundary effects and analyze its magnon-magnon correlations, marking A, B and C in figure 5(a). As shown in figures 5(b), (c) and (d), almost all of the magnons are distributed among the next-minor-diagonal lines in the magnon-magnon correlation. These results follow from the circumstance that two strongly NNN interacting magnons initially occupying the NNN sites form a bound pair and tunnel together on the spin chain. These time evolved results are in agreement with our

analytical predictions. The two-magnon quantum walks pave the way for experimentally verifying whether the modulation-induced long-range bound states exist or not.

6. Summary and Discussion

Based on the state-of-art techniques of ultracold atomic experiments, our model can be experimentally simulated with ultracold two-level atoms in one-dimensional optical lattices. We have presented a scheme for generating tunable long-range magnon bound states by introducing a gradient magnetic field and time-modulated hopping into the ultracold atomic systems. Taking advantage of the flexible tunability, desired long-range bound states can be engineered by changing the modulated parameters and the interaction strength Δ tuned by Feshbach resonance. The prerequisite lies in the modulation frequency ω is equal to the magnetic field gradient B , which enables a single magnon to tunnel resonantly onto its neighbors. It can be understood as the phonon-assisted tunneling among the spin chain. We not only analyze the correlation properties of modulation-induced long-range bound states, but also explore the interplay between the original and modulation-induced bound states with the changing of NN interaction. Further, we obtain an effective two-magnon model via a many-body perturbation theory to interpret the origin and condition for the remarkable long-range bound states. The effective two-magnon model becomes invalid near the resonant point $\Delta = \omega$, where resonance between the two types of bound states happens. In addition, two-magnon quantum walks can be used as an experimental verification of modulation-induced long-range bound states. Our scheme is not limited to two-magnon systems, and also gives insights into engineering novel states of matter of multi-particle Floquet systems.

A few promising questions remain open and motivate further investigations. For example, this proposed scheme has potential to realize the fractional topological states which exist in the one-dimensional superlattice with the dipole-dipole interactions [51]. By introducing the modulation-induced NNN interaction, the competitive relation between two kinds of bound states may bring different topological effects in periodically modulated NN-interaction spin chain. In the whole text, we focus on the analysis in the high-frequency region, while more abundant phenomenons may arise in the low-frequency one.

7. Acknowledgements

This work is supported by the Key-Area Research and Development Program of Guangdong Province under Grants No. 2019B030330001, the National Natural Science Foundation of China (NNSFC) under Grants [No. 11874434, No. 11574405], and the Science and Technology Program of Guangzhou (China) under Grants No. 201904020024. Y.K. is partially supported by the Office of China Postdoctoral Council (Grant No. 20180052), the National Natural Science Foundation of China (Grant No. 11904419), and the Australian Research Council (DP200101168).

Appendix A. Longer-range bound states

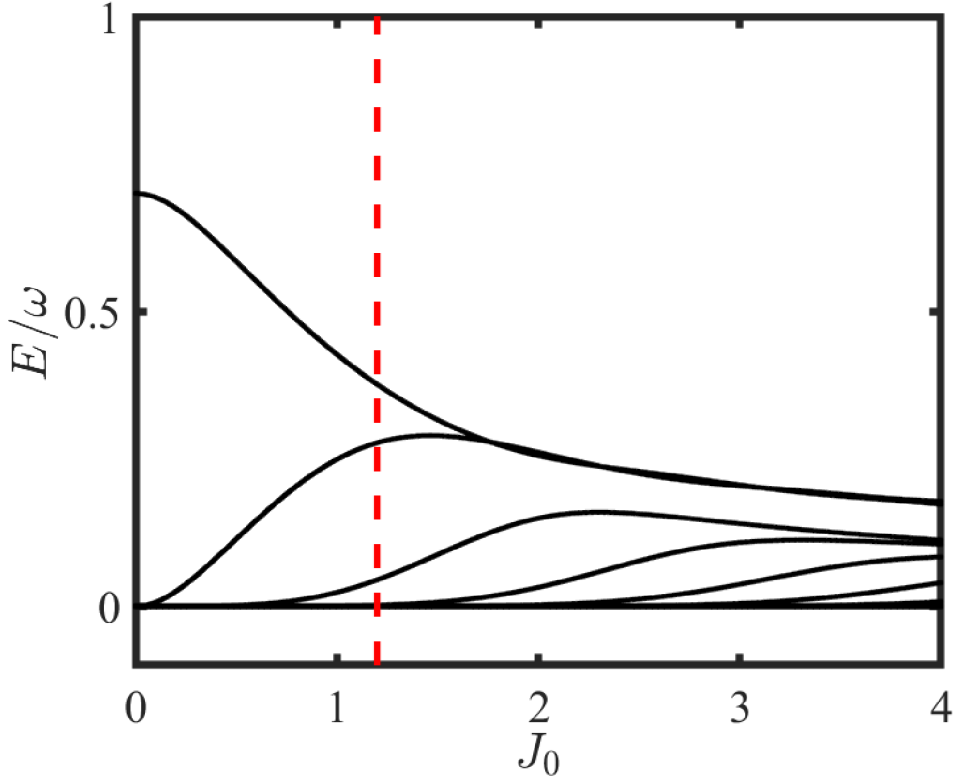


Figure A1. (Color online) Quasienergy spectrum E vs. J_0 . We diagonalize the Floquet-Bloch lattice model (12) with $\omega = B = 1$, $\Delta = 0.7$ and $J_1 = 0.001$. The red dashed line corresponds to $J_0 = 1.2$.

Our system not only is able to induce NNN bound states, but also has potential to engineer longer-range bound states. In figure A1, we show how the quasienergy changes with J_0 . With the increase of J_0 , more and more modulation-induced bands emerge. To illustrate how the longer-range bound state is induced, we take $J_0 = 1.2$ marked with red dashed line in figure A1 as an example. We obtain the two-body Floquet-Bloch bands versus K by solving the eigenequation (15) in figure A2. The parameters are chosen as $\omega = B = 1$, $\Delta = 0.7$, $J_0 = 1.2$ and $J_1 = 0.001$. Four isolated bands appear above the continuum band in figure A2. We respectively mark the Floquet states from different isolated bands as I, II, III and IV in the quasienergy spectrum and analyze their correlated properties in the insets I, II, III and IV of figure A2. The magnon-magnon correlations clearly show that, aside from NN and NNN bound states, the bound state with relative distance at three and four sites appear. It is worth noting that these correlations mostly distributes along their corresponding diagonal lines and partly distribute in other diagonal lines, called as hybridization. According to our further numerical results, in the appearance of modulation-induced longer-range bound state, hybridization inevitably arises and even more complex case, e.g., the transformation between different types of bound state in the same bound-state band.

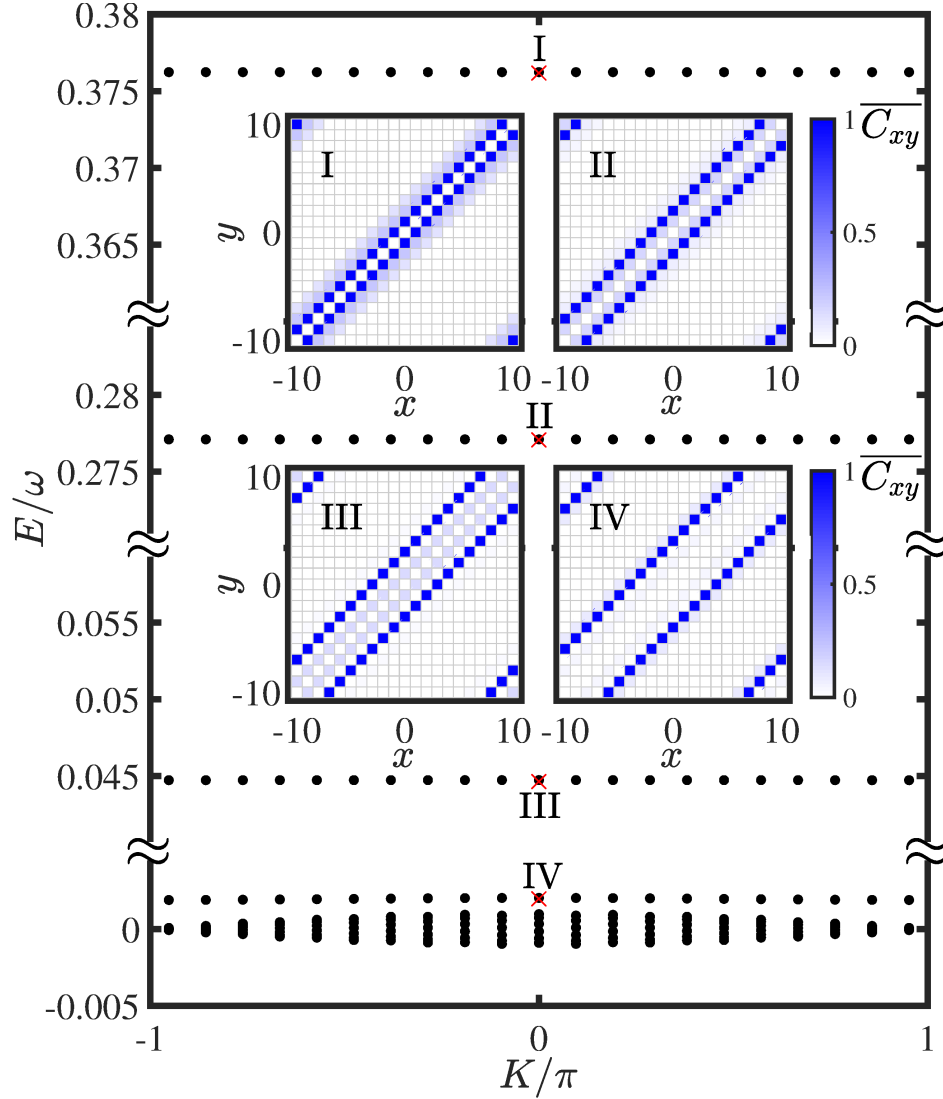


Figure A2. (Color online) Quasienergy spectrum E vs. K . The insets I, II, III and IV respectively describe the normalized magnon-magnon correlations $\overline{C_{xy}} = C_{xy}/C_{xy}^{max}$ of Floquet states labeled in the four bound-state band above the continuum band. The parameters are chosen as $\omega = B = 1$, $\Delta = 0.7$, $J_0 = 1.2$ and $J_1 = 0.001$.

References

- [1] Bukov M, D'Alessio L and Polkovnikov A 2015 Universal high-frequency behavior of periodically driven systems: from dynamical stabilization to Floquet engineering *Adv. Phys.* **64** 139
- [2] Ke Y, Qin X, Kivshar Y S and Lee C 2017 Multiparticle Wannier states and Thouless pumping of interacting bosons *Phys. Rev. A* **95** 063630
- [3] Li Z -Z, Lam C -H and You J Q 2017 Floquet engineering of long-range p -wave superconductivity: Beyond the high-frequency limit *Phys. Rev. B* **96** 155438
- [4] Görg F, Messer M, Sandholzer K, Jotzu G, Desbuquois R and Esslinger T 2018 Enhancement and sign change of magnetic correlations in a driven quantum many-body system *Nature* **553** 481
- [5] Wang B, Ünal F N and Eckardt A 2018 Floquet Engineering of Optical Solenoids and Quantized

- Charge Pumping along Tailored Paths in Two-Dimensional Chern Insulators *Phys. Rev. Lett.* **120** 243602
- [6] Li L, Lee C H and Gong J 2018 Realistic Floquet Semimetal with Exotic Topological Linkages between Arbitrarily Many Nodal Loops *Phys. Rev. Lett.* **121** 036401
 - [7] Lee C H, Li G, Jin G, Liu Y and Zhang X 2018 Topological dynamics of gyroscopic and Floquet lattices from Newton's laws *Phys. Rev. B* **97** 085110
 - [8] Rudner M S and Lindner N H 2019 Floquet topological insulators: from band structure engineering to novel non-equilibrium quantum phenomena arXiv: 1909.02008
 - [9] Dal Lago V, Atala M and Foa Torres L E F 2015 Floquet topological transitions in a driven one-dimensional topological insulator *Phys. Rev. A* **92** 023624
 - [10] Zhu B, Zhong H, Ke Y, Qin X, Sukhorukov A A, Kivshar Y S and Lee C 2018 Topological Floquet edge states in periodically curved waveguides *Phys. Rev. A* **98** 013855
 - [11] Zheng W and Zhai H 2014 Floquet topological states in shaking optical lattices *Phys. Rev. A* **89** 061603
 - [12] Holthaus M 2015 Floquet engineering with quasienergy bands of periodically driven optical lattices *J. Phys. B: At. Mol. Opt. Phys.* **49** 013001
 - [13] Lohse M, Schweizer C, Zilberberg O, Aidelsburger M and Bloch I 2016 A Thouless quantum pump with ultracold bosonic atoms in an optical superlattice *Nat. Phys.* **12** 350
 - [14] Nakajima S, Tomita T, Taie S, Ichinose T, Ozawa H, Wang L, Troyer M and Takahashi Y 2016 Topological Thouless pumping of ultracold fermions *Nat. Phys.* **12** 296
 - [15] Ke Y, Qin X, Mei F, Zhong H, Kivshar Y S and Lee C 2016 Topological phase transitions and Thouless pumping of light in photonic waveguide arrays *Laser Photon. Rev.* **10** 995
 - [16] Zilberberg O, Huang S, Guglielmon J, Wang M, Chen K P, Kraus Y E and Rechtsman M C 2018 Photonic topological boundary pumping as a probe of 4D quantum Hall physics *Nature* **553** 59
 - [17] Lohse M, Schweizer C, Price H M, Zilberberg O and Bloch I 2018 Exploring 4D quantum Hall physics with a 2D topological charge pump *Nature* **553** 55
 - [18] Hu S, Ke Y, Deng Y and Lee C 2019 Dispersion-suppressed topological Thouless pumping *Phys. Rev. B* **100** 064302
 - [19] Goldman N and Dalibard J 2014 Periodically Driven Quantum Systems: Effective Hamiltonians and Engineered Gauge Fields *Phys. Rev. X* **4** 031027
 - [20] Tenenbaum Katan Y and Podolsky D 2013 Modulated Floquet Topological Insulators *Phys. Rev. Lett.* **110** 016802
 - [21] Cayssol J, Dóra B, Simon F and Moessner R 2013 Floquet Topological Insulators *Phys. Status Solidi RRL* **7** 101
 - [22] Rechtsman M C, Zeuner J M, Plotnik Y, Lumer Y, Podolsky D, Dreisow F, Nolte S, Segev M and Szameit A 2013 Photonic Floquet topological insulators *Nature* **496** 196
 - [23] Gomez-Leon A and Platero G 2013 Floquet-Bloch Theory and Topology in Periodically Driven Lattices *Phys. Rev. Lett.* **110** 200403
 - [24] Clark L W, Gaj A, Feng L and Chin C 2017 Collective emission of matter-wave jets from driven Bose-Einstein condensates *Nature* **551** 356
 - [25] Eckardt A 2017 Colloquium: Atomic quantum gases in periodically driven optical lattices *Rev. Mod. Phys.* **89** 011004
 - [26] Widera A, Mandel O, Greiner M, Kreim S, Hänsch T W and Bloch I 2004 Entanglement Interferometry for Precision Measurement of Atomic Scattering Properties *Phys. Rev. Lett.* **92** 160406
 - [27] Gross C, Zibold T, Nicklas E, Estève J and Oberthaler M K 2010 Nonlinear atom interferometer surpasses classical precision limit *Nature* **464** 1165
 - [28] Anisimovas E, Žlabys G, Anderson B M, Juzeliūnas G and Eckardt A 2015 Role of real-space micromotion for bosonic and fermionic Floquet fractional Chern insulators *Phys. Rev. B* **91** 245135
 - [29] Cardarelli L, Greschner S and Santos L 2016 Engineering interactions and anyon statistics by

- multicolor lattice-depth modulations *Phys. Rev. A* **94** 023615
- [30] Zhao Z, Knolle J and Mintert F 2019 Engineered nearest-neighbor interactions with doubly modulated optical lattices *Phys. Rev. A* **100** 053610
 - [31] Lee C, Ho W, Yang B, Gong J and Papić Z 2018 Floquet Mechanism for Non-Abelian Fractional Quantum Hall States *Phys. Rev. Lett.* **121** 237401
 - [32] Meinert F, Mark M J, Lauber K, Daley A J and Nägerl H -C 2016 Floquet Engineering of Correlated Tunneling in the Bose-Hubbard Model with Ultracold Atoms *Phys. Rev. Lett.* **116** 205301
 - [33] Clark L W, Anderson B M, Feng L, Gaj A, Levin K and Chin C 2018 Observation of Density-Dependent Gauge Fields in a Bose-Einstein Condensate Based on Micromotion Control in a Shaken Two-Dimensional Lattice *Phys. Rev. Lett.* **121** 030402
 - [34] Fukuhara T, Kantian A, Endres M, Cheneau M, Schauß P, Hild S, Bellem D, Schollwöck U, Giamarchi T, Gross C, Bloch I and Kuhr S 2013 Quantum dynamics of a mobile spin impurity *Nat. Phys.* **9** 235
 - [35] Fukuhara T, Schauß P, Endres M, Hild S, Cheneau M, Bloch I and Gross C 2013 Microscopic observation of magnon bound states and their dynamics *Nature* **502** 76
 - [36] Qin X, Mei F, Ke Y, Zhang L and Lee C 2018 Topological invariant and cotranslational symmetry in strongly interacting multi-magnon systems *New. J. Phys.* **20** 013003
 - [37] Amato-Grill J, Jepsen N, Dimitrova I, Lunden W and Ketterle W 2019 Interaction spectroscopy of a two-component Mott insulator *Phys. Rev. A* **99** 033612
 - [38] Dimitrova I, Jepsen N, Buyskikh A, Venegas-Gomez A, Amato-Grill J, Daley A and Ketterle W 2020 Enhanced Superexchange in a Tilted Mott Insulator *Phys. Rev. Lett.* **124** 043204
 - [39] Lee T 2016 Floquet engineering from long-range to short-range interactions *Phys. Rev. A* **94** 040701
 - [40] Buchleitner A and Kolovsky A R 2003 Interaction-Induced Decoherence of Atomic Bloch Oscillations *Phys. Rev. Lett.* **91** 253002
 - [41] Kolovsky A and Buchleitner A 2003 Floquet-Bloch operator for the Bose-Hubbard model with static field *Phys. Rev. E* **68** 056213
 - [42] Liu W, Ke Y, Zhang L and Lee C 2019 Bloch oscillations of multimagnon excitations in a Heisenberg XXZ chain *Phys. Rev. A* **99** 063614
 - [43] Tarallo M G, Alberti A, Poli N, Chiofalo M L, Wang F -Y and Tino G M 2012 Delocalization-enhanced Bloch oscillations and driven resonant tunneling in optical lattices for precision force measurements *Phys. Rev. A* **86** 033615
 - [44] Ivanov V V, Alberti A, Schioppo M, Ferrari G, Artoni M, Chiofalo M L and Tino G M 2008 Coherent Delocalization of Atomic Wave Packets in Driven Lattice Potentials *Phys. Rev. Lett.* **100** 043602
 - [45] Teichmann N, Esmann M and Weiss C 2009 Fractional photon-assisted tunneling for Bose-Einstein condensates in a double well *Phys. Rev. A* **79** 063620
 - [46] Ma R, Tai M E, Preiss P M, Bakr W S, Simon J and Greiner M 2011 Photon-Assisted Tunneling in a Biased Strongly Correlated Bose Gas *Phys. Rev. Lett.* **107** 095301
 - [47] Qin X, Ke Y, Guan X, Li Z, Andrei N and Lee C 2014 Statistics-dependent quantum co-walking of two particles in one-dimensional lattices with nearest-neighbor interactions *Phys. Rev. A* **90** 062301
 - [48] Bravyi S, DiVincenzo D P and Loss D 2011 Schrieffer-Wolff transformation for quantum many-body systems *Ann. Phys.* **326** 2793
 - [49] Takahashi M 1977 Half-filled Hubbard model at low temperature *J. Phys. C* **10** 1289
 - [50] Lee C 2004 Bose-Einstein Condensation of Particle-Hole Pairs in Ultracold Fermionic Atoms Trapped within Optical Lattices *Phys. Rev. Lett.* **93** 120406
 - [51] Xu Z, Li L and Chen S 2013 Fractional Topological States of Dipolar Fermions in One-Dimensional Optical Superlattices *Phys. Rev. Lett.* **110** 215301